Influence of the airborne sound sensor position on the detectability of acoustic emissions during deep penetration laser welding

Andreas Krämer[1,a)], Ronald Pordzik[1,b)], Thorsten Mattulat[1,c)]
[1)] BIAS - Bremer Institut für angewandte Strahltechnik GmbH, Bremen, Deutschland

Abstract
Zur Überwachung von Laserstrahlschweißprozessen und zur Erkennung bzw. aktiven Vermeidung von Prozessfehlern können neben optischen Messverfahren wie der Pyrometrie auch akustische Verfahren genutzt werden. Um Prozessereignisse zuverlässig zu erfassen, ist es unabdingbar, die jeweiligen Sensoren so zu positionieren, dass spezifische Signalcharakteristika reproduzierbar und signifikant detektierbar sind. Gegenwärtig gibt es wenige Untersuchungen hinsichtlich der gezielten Positionierung von Luftschallsensoren, insbesondere für Prozessemissionen im Ultraschallbereich. In dieser Untersuchung wird daher der Einfluss des Prozessabstandes sowie des Anstellwinkels und der Orientierung des Mikrofons zum Keyhole während eines Laserstrahltiefschweißprozesses hinsichtlich der frequenzaufgelösten Detektierbarkeit von akustischen Emissionen untersucht. Es wird gezeigt, dass für einen breiten Ultraschallbereich ein flacher Winkel des Sensors bezogen auf die Probenoberfläche zu einer höheren Signalstärke der akustischen Emissionen gegenüber steilen Winkeln führt.

For monitoring laser beam welding processes and detecting or actively avoiding process defects, acoustic based measurements can be used in addition to optical measurement methods such as pyrometry. To reliably detect process events, it is essential to position the respective sensors in such a way that specific signal characteristics are reproducible and significant. However, there are only few investigations regarding the positioning for airborne sound sensors, especially for the detection of process emissions in the ultrasonic range. Therefore, in this research, the influence of the process distance as well as the angle and orientation of the microphone to a laser beam deep penetration welding process is investigated with respect to the detectability of process emissions in different frequency bands. It is shown that for a wide ultrasonic range a flat sensor angle with respect to the sample surface leads to an increased signal strength of the acoustic emissions compared to steep angles.

1. Introduction

Laser beam welding is a widespread joining technique that allows for high welding speeds, high seam qualities and low heat-affected zones. A distinction must be made between heat conduction welding and deep penetration welding. In heat conduction welding mode, the laser power is absorbed at the surface by Fresnel absorption. The heat spreads out into the material volume by thermal conduction and the material melts in the vicinity of the laser beam, forming circular weld cross-sections [1]. Deep penetration welding, on the other hand, exceeds a threshold intensity, causing the material to vaporize and form a keyhole with a high aspect ratio [1]. While there have been initial researches regarding the correlation of acoustic emissions and heat conduction welding [2], most studies have focused on the acoustic process emissions during laser deep penetration welding. The objective of these studies was to gain an understanding of the origin of acoustic process emissions and to obtain process information that can be correlated with process defects. In addition to structure-borne sound sensors, airborne sound sensors have also been used. For example, Duley et al. investigated acoustic emissions during laser beam welding of Al 1100 and were able to identify characteristic acoustic spectra, as well as a dependence on surface oxide contamination [3]. Mao et al. showed that the acoustic emissions become stronger during the transition from heat conduction welding to deep penetration welding and that there is a correlation between optical and acoustic emission in the low frequency spectrum due to plasma fluctuation [4]. Bastuck set up a model regarding sound generation within deep penetration welding processes and concluded that, in addition to the keyhole as a sound source, parts of the acoustic emissions are generated by evaporation of the surface coatings [5]. Furthermore, he demonstrated the suitability of the acoustic emission detection for process monitoring with respect to decoating processes and full penetration welding. Yusof et al. used synchronized wavelet analysis to improve the classification of airborne sound data into different process regimes [6]. More recently, machine-learning approaches have also been pursued. For example, Tomcic et al. introduced a total of 17 acoustic parameters to analyze which of these parameters were significant for predicting weld penetration depth using Gaussian process regression [7]. Although the authors of these studies developed explanatory approaches regarding the origin of the acoustic process emissions, there is currently no conclusive model. One challenge they faced, in addition to statistical signal fluctuation and the influence of noise, was the strong dependence on sensor positioning [6].

This dependence implies that the position of the airborne sound sensors must be carefully chosen. However, there is no uniform approach between the authors. Thus, in addition to the frequency ranges considered, the distances to the process zone vary by a factor of 12, as do the angles of attack, ranging from 30 ° to 90 °. Frequently, there is also no precise information on the position itself or on the selection process of the position. This severely impairs the reproducibility and thus the transferability of the findings. It's important to note, that the positional sensitivity of airborne sound sensors differ depending on their physical working principle.

The present study therefore aims to investigate on the influence of the sensor position on the signal quality of an exemplary airborne sound sensor, the XARION Eta250, for monitoring laser beam welding processes.

2. Experimental setup and methods

To investigate the influence of the sensor position on the signal quality, welding experiments in different metals were conducted. The distance of the airborne sound sensor to the keyhole opening as well as the angle of attack in relation to the specimen surface and the orientation, trailing or leading the process, were varied. The distance was varied between 100 mm and 200 mm, the angle of attack between 15 °, 45 ° and 65 °. The exact positioning was accomplished using a perforated plate, allowing the airborne sound sensor to be mounted at defined positions, as can be seen in Figure 1.

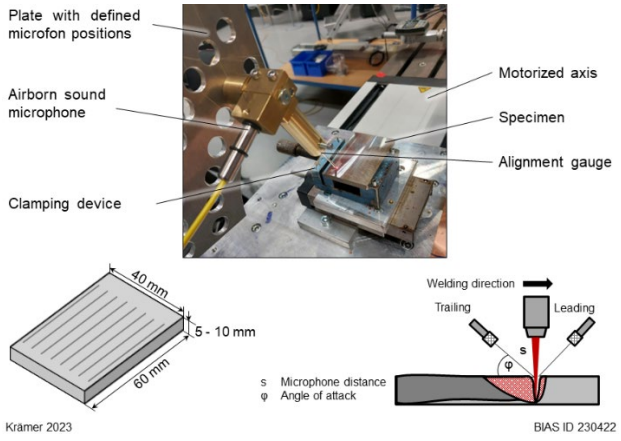

Figure 1: Experimental setup

An Eta250 Ultra microphone (XARION) was used as airborne sound sensor. The frequency range of the microphone ranges from 10 Hz to 1 MHz. The microphone uses a Fabry-Pérot interferometer as working principle. The sound pressure changes the refractive index of the air which changes the optical wavelength of light propagation through the pressure waves. These alternations change the interferences within the interferometer cavity, which are detected by a photodiode and thus leading to changes in the electrical signal [8]. Since the sensor head consists of the Fabry-Pérot cavity, the sensor shows a directive dependence regarding the alignment of the sensor head towards the sound source. Therefore, an alignment gauge was used to align the sensor towards the pilot laser and thus the subsequent keyhole opening.

Data acquisition was performed without further signal amplification using the NI cRIO-9035 and the NI-9222 module (both National Instruments Corp.) with a sampling rate of 500 kHz. This limited the maximum detectable frequency of the acoustic process emissions to 250 kHz according to the Nyquist-Shannon sampling theorem. Using sliding Fast Fourier Transformations, the time resolved spectrum of frequencies can be calculated, resulting in a 3D acoustic spectrogram. The length of the sliding window in which the individual FFTs were calculated was 2048 µs and the overlap between neighboring windows was 256 µs.

To determine the acoustic energy in defined frequency bands, the spectrogram is integrated along the selected frequency range for each time step. This provides a time-resolved acoustic energy within defined frequencies. Furthermore, to analyze the acoustic emissions excited by the process, the power spectral density was calculated over the entire recording duration using Welch's method [9]. Here, a window size of 10 ms and an overlap of 5 ms were used.

The laser source used was the TruDisk12002 disk laser (TRUMPF) operating at a wavelength of 1030 nm. The fixed BEO D70 laser optics (TRUMPF) was connected to the laser source using a 600 µm fiber. The focal diameter measured with the MSM + HBHP (PRIMES) was 576 µm.

Five seams were welded per microphone position. On a single specimen, 8 different seams were welded, each with a different sensor position and after the complete cooling to room temperature. Two different materials were used to investigate the material influence: 2.4068 nickel and 1.0122 mild steel, whose chemical compositions can be found in table 1 and table 2. The specimen dimensions were 60x40x5 mm³ for nickel and 60x40x10 mm³ for steel. The specimens were clamped and moved via an axis that provided a constant welding speed of 2.4 m/min. To ensure comparability, an identical welding depth of 2 mm was used. For this purpose, seams were first welded with different laser powers and then metallographic cross sections were analyzed to determine the respective weld penetration depth. Subsequently, the necessary laser powers for achieving the required weld depth were determined by means of linear interpolation. The laser power used to achieve the weld penetration depth was 2400 W for nickel and 1890 W for steel.

Table 1: Chemical composition of 2.4068 nickel

Ni	Fe	Co	Mn	C	Cu	Mg	Ti
99,48	0,22	0,02	0,02	0,02	0,01	0,01	0,01

Table 2: Chemical composition of 1.0122 mild steel

Fe	C	Si	Mn	P	S	Cr	Ni
98,57	0,08	0,20	0,52	0,01	0,02	0,16	0,13

3. Results

The recorded raw signal of the airborne sound microphone can be transformed into a spectrogram of the acoustic emissions by means of Fourier transformation. The spectrogram shown in Figure 2 shows the emissions from a single seam in nickel. The start of the process is clearly observable at about 0.1 s. Ambient noise from the shielding gas and axis motion, each of which can be viewed in isolation before and after the process, exhibits only low emissions in the non-ultrasonic range.

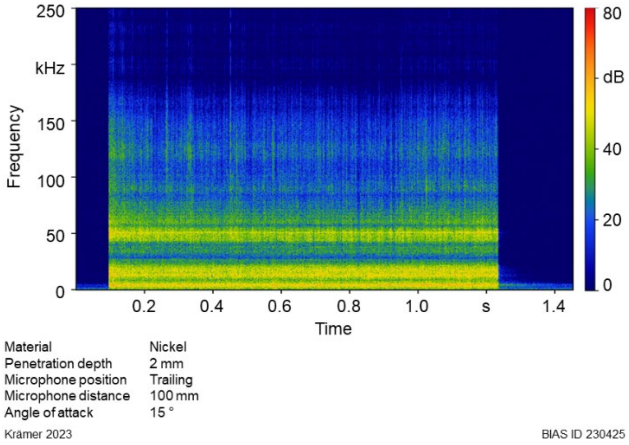

Figure 2: Acoustic 3D spectrogram of a single seam in nickel

Figure 3 shows the power spectral densities (PSDs) acquired from different angles of attack of the airborne sound sensor at constant distance from the process zone for seams in nickel according to the methodology described in section 2. The PSD decreases with increasing frequency. However, a narrow peak at 8 kHz is initially noticeable, as well as broadband peaks at 15 kHz and 50 kHz. Likewise, an additional very prominent narrowband peak at 50 kHz stands out.

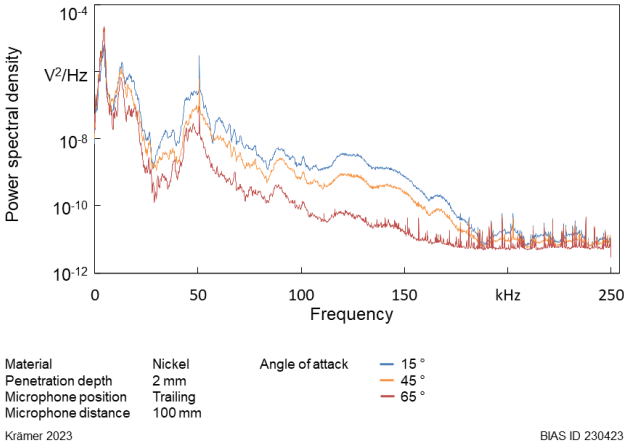

Figure 3: PSDs of seams in nickel depending on the angle of attack

For frequencies above 15 kHz, it can be determined that the signal intensity decreases with increasing angle of attack. Furthermore, single peaks increasingly appear for an angle of 65 ° from 150 kHz on.

Figure 4 shows, due to the higher resolution of the low-frequency ranges, that for frequencies below 10 kHz an angle of attack of 65 ° leads to higher signal intensities compared to 15 °. It is also clear that the narrowband peaks at 50 kHz occur at the exact same frequency regardless of the angle of attack.

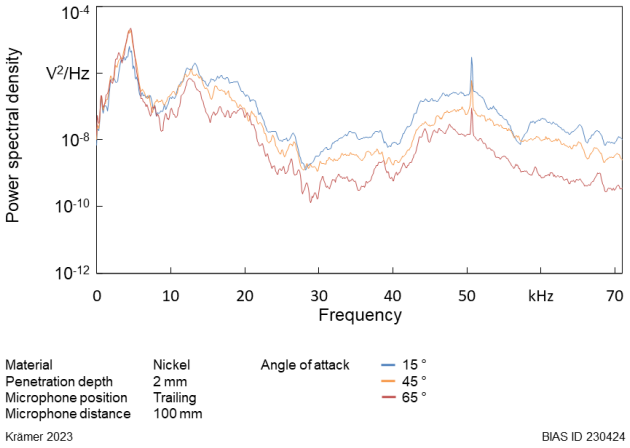

Figure 4: PSDs of seams in nickel depending on the angle of attack, lower frequencies

Regarding the orientation of the airborne microphone, it can be seen in Figure 5 that for frequencies above 100 kHz no differences are apparent as to whether the microphone is trailing or leading the process. Between 25 kHz and 100 kHz, however, an orientation leading the process results in higher signal intensities.

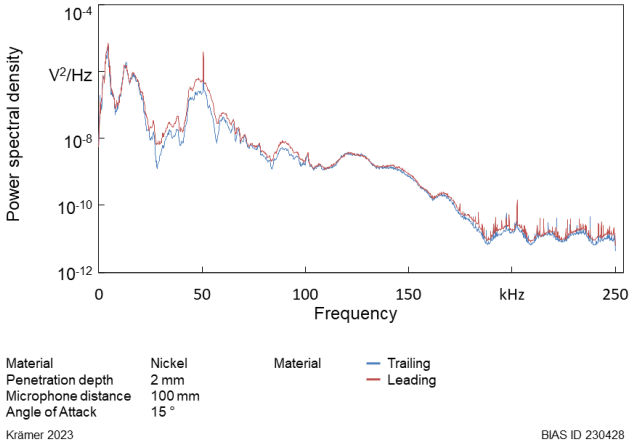

Figure 5: PSDs of seams in nickel depending on the orientation

When the quotient of PSDs of the recordings with angles of attack of 15 ° and 65 ° is formed, as displayed in Figure 6, it becomes clear that the percentage differences increase with increasing frequency. However, a convergence between both signals at 80 kHz as well as only small differences for frequencies above 175 kHz are observed.

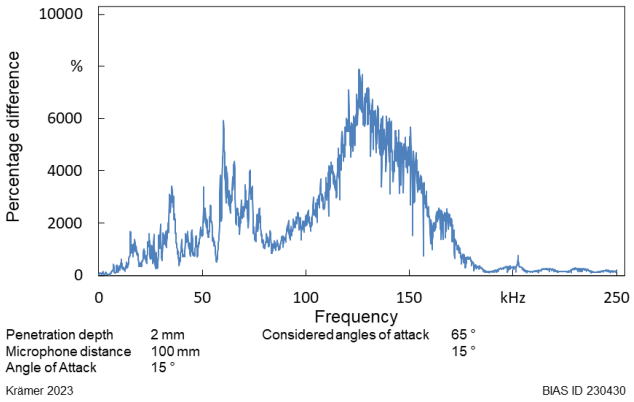

Figure 6: Quotient of the PSDs from an angle of attack of 15 ° and 65 °

Subsequent investigations into the transferability of the angle of attack to another alloy have shown that higher signal intensities are also achieved for seams in steel for frequencies above 15 kHz when the airborne sound sensor is positioned at a flat angle, as can be seen in Figure 7.

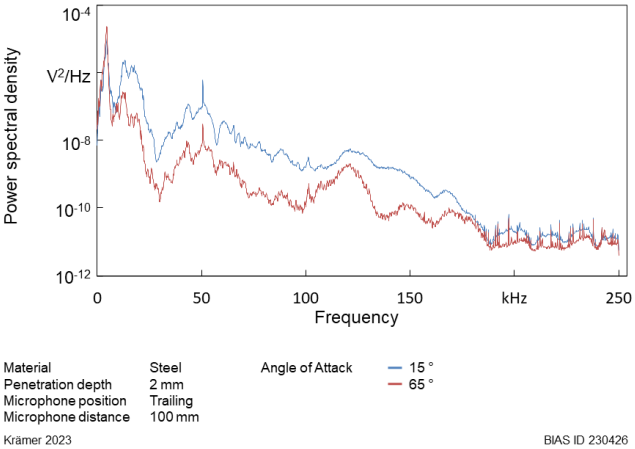

Figure 7: PSDs for seams in steel depending on the angle of attack

A direct comparison of the power spectral density of seams in nickel and steel, each with an identical sensor position, is shown in Figure 8. A high similarity of the curves stands out.

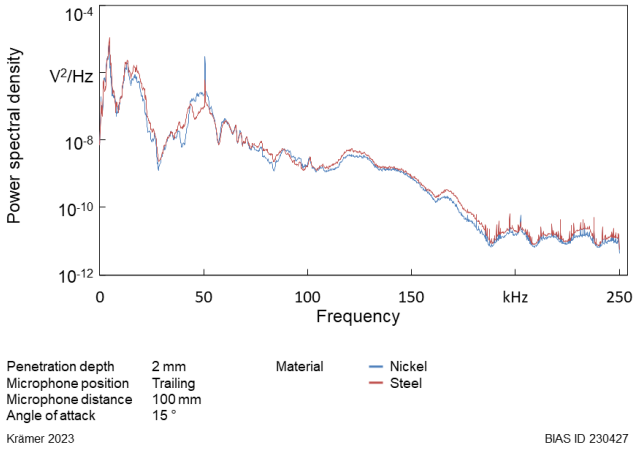

Figure 8: PSDs for seams in nickel and steel for identical sensor positions

Almost identical values can be observed over most frequency ranges. However, significant differences appear in the broadband peak at 50 kHz. Initially, the signal intensity for the seam in nickel drops at about 48 kHz, while the intensity for steel increases here. However, as the peak progresses, the power density for nickel significantly exceeds the PSD for steel. For both materials, however, a narrowband, prominent peak occurs at the same frequency at about 50 kHz.

Figure 9 shows the acoustic energy for the frequency band of 50 kHz to 100 kHz for a trailing and leading position of the sensor for welds in nickel, with equal distances and angles of attack in each case. The data range considered starts at 0.4 s to exclude the effects of process start. The acoustic energy for the leading orientation is significantly higher than for the trailing position. Linear regressions indicate that the energy decreases with increasing process duration in the case of the leading orientation, while it increases in the case of the trailing position. The same behavior can be observed for steel. However, for the frequency band of 100 kHz to 150 kHz, the acoustic energy for both positions increase with increasing process duration.

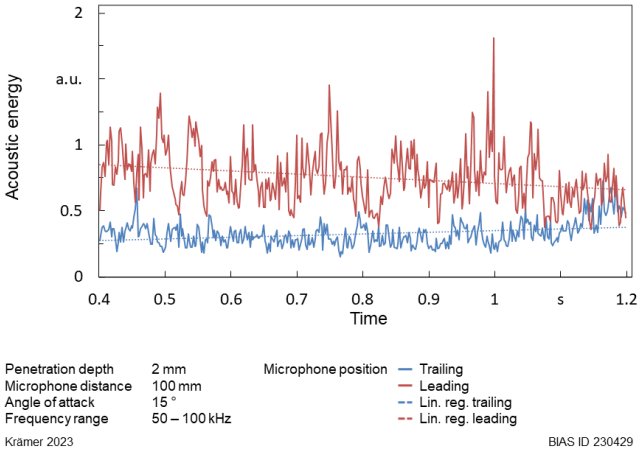

Figure 9: Acoustic energy from 50 – 100 kHz for different orientations in nickel

4. Discussion

In general, during welding with the parameters used, the entire acoustic frequency spectrum under consideration up to 250 kHz is excited of which the frequencies up to 10 kHz exhibit the most pronounced excitations, while the frequencies above 175 kHz are only slightly excited. The prominent narrowband peak at 50 kHz is probably due to relaxation oscillations of the disk laser used. It should also be noted that in low-frequency bands, noise from the axis movement and the shielding gas flow are contained.

As already observed by Yusof et al. [6], the signal intensity strongly depends on the positioning of the sensor. The results show that a low angle of attack with respect to the specimen surface leads to significantly stronger signals for frequencies higher than 10 kHz. This could be observed for nickel as well as for steel. According to

Bastuck's model the acoustic process emissions during laser beam welding originate from surface evaporations due to advancing heat as well as from the keyhole itself [5]. However, since neither of the materials considered has a coating, this effect can be neglected. Accordingly, the origin of the sound can essentially be attributed to the process zone. As Bastuck showed by using structure-borne sound sensors, deep penetration welding is accompanied by strong structure-borne sound emissions, which means that the component itself is mechanically excited by the process. However, the mechanical vibration of the component also excites the ambient air, thus emitting secondary-order airborne sound. This principle is also used in non-destructive ultrasonic testing systems for weld seams. When sound is propagating through air, the sound pressure is attenuated by various effects. As Bass et al. describe, this attenuation depends not only on temperature, humidity and ambient pressure, but also in particular on the distance to the sound source and the sound frequency [10]. The relationship between the distance to the sound source and the sound pressure is exponential.

Due to a flat angle of attack to the specimen surface, the distance to the process remains identical, but the airborne sound sensor is located closer to the vibrating specimen. The higher sound pressure causes stronger signal amplitudes in the sensor. It must also be taken into account that a flat angle of attack increases the angle between the perpendicular axis of the sensor head and the surface of the specimen. Since the microphone is sensitive regarding the angle towards the sound source this effect has to be considered.

The higher sound pressure however is indicated in the differences of the time resolved acoustic energies depending on the orientation of the airborne sound microphone to the process zone. As can be seen in Figure 9, the acoustic energy decreases in the case of a leading position, while it increases for a trailing position. In a trailing position the sensor is not directly above the specimen. As the process is running, the microphone approaches the sample. This implies that the sensor is closer to the source of secondary-order airborne sound while the distance to the keyhole opening hasn't changed. However, if the sensor is oriented in a leading orientation, it moves away from sample as the process progresses.

Also, considering the differences in power spectral densities as a function of frequency for a steep and flat angle of attack it's indicated that, according to the frequency-dependent attenuation described by Bass et al [9], the airborne microphone must be closer to a sound source in the case of a flat angle of attack.

5. Conclusion

The investigations into the positioning of the airborne sound microphone have shown that a flat angle of attack of the sensor relative to the sample surface leads to an increased signal strength of the acoustic process emissions in a wide ultrasonic range compared to steep angles. Likewise, it can be observed that positioning the microphone in front of the process leads to a small signal increase.

Acknowledgement

The project on which this publication is based was funded by the German Federal Ministry of Education and Research under grant number 03HY119F.The responsibility for the contents of the publication lies with the authors.

Contact

Andreas Krämer
BIAS – Bremer Institut für angewandte Strahltechnik GmbH
Klagenfurter Straße 5
28359 Bremen

[a] kraemer@bias.de, ORCID: 0009-0003-8023-0788

[b] pordzik@bias.de, ORCID: 0000-0002-7753-9579

[c] mattulat@bias.de, ORCID: 0000-0002-6964-1565

References

[1] J. Bliedtner, H. Müller, and A. Barz, *Lasermaterialbearbeitung: Grundlagen – Verfahren – Anwendungen – Beispiele*. München: Hanser, 2013.

[2] N. Authier, E. Touzet, F. Lücking, R. Sommerhuber, V. Bruyere, and P. Namy, "Coupled membrane free optical microphone and optical coherence tomography keyhole measurements to setup welding laser parameters," *High-Power Laser Materials Processing: Applications, Diagnostics, and Systems IX*, p. 8, 2020, doi: 10.1117/12.2543999.

[3] W. W. Duley and Y. L. Mao, "The effect of surface condition on acoustic emissions during welding of aluminium with CO2 laser radiation," *Journal of Physics D: Applied Physics*, vol. 27, pp. 1379–1383, 1994.

[4] Y.-L. Mao, G. Kinsman, and W. W. Duley, "Real-Time Fast Fourier Transform Analysis of Acoustic Emission during CO 2 Laser Welding of Materials," *Journal of Laser Applications*, vol. 5, no. 2, pp. 17–22, 1993, doi: 10.2351/1.4745326.

[5] M. Bastuck, "In-Situ-Überwachung von Laserschweißprozessen mittels höherfrequenter Schallemissionen," Dissertation, Universität des Saarlandes, 2016.

[6] M. Yusof, M. Ishak, and M. F. Ghazali, “Classification of weld penetration condition through synchrosqueezed-wavelet analysis of sound signal acquired from pulse mode laser welding process,” *Journal of Materials Processing Technology*, vol. 279, p. 116559, 2020, doi: 10.1016/j.jmatprotec.2019.116559.

[7] L. Tomcic, A. Ederer, S. Grabmann, M. Kick, J. Kriegler, and M. F. Zaeh, “Interpreting acoustic emissions to determine the weld depth during laser beam welding,” *Journal of Laser Applications*, vol. 34, no. 4, 2022, doi: 10.2351/7.0000796.

[8] B. Fischer, W. Rohringer, N. Panzer, and S. Hecker, “Acoustic Process Control for Laser Material Processing,” *Laser Technik Journal*, vol. 14, no. 5, pp. 21–25, 2017, doi: 10.1002/latj.201700029.

[9] P. Welch, “The use of fast Fourier transform for the estimation of power spectra: A method based on time averaging over short, modified periodograms,” *IEEE Trans. Audio Electroacoust.*, vol. 15, no. 2, pp. 70–73, 1967, doi: 10.1109/TAU.1967.1161901.

[10] H. E. Bass, L. C. Sutherland, A. J. Zuckerwar, D. T. Blackstock, and D. M. Hester, “Atmospheric absorption of sound: Further developments,” *The Journal of the Acoustical Society of America*, vol. 97, no. 1, 1995, doi: 10.1121/1.412989.